STEM CELLS AND DEVELOPMENT
Volume 28, Number 19, 2019

DOI: 10.1089/scd.2019.0104

Investigation of Postnatal Craniofacial Bone Development with Tissue Clearing-Based Three-Dimensional Imaging

Wenjing Luo,[1] Yating Yi,[2,3] Dian Jing,[2,3] Shiwen Zhang,[3]
Yi Men,[2] Woo-Ping Ge,[4–7] and Hu Zhao[2]

Traditional two-dimensional histological sections and microcomputed tomography remain to be the major tools for studying craniofacial bones despite the complicated spatial organization of craniofacial organs. Recently, our laboratory developed the Poly(Ethylene Glycol) Associated Solvent System (PEGASOS) tissue clearing method, which can efficiently render hard tissues, including bones and teeth fully transparent without losing endogenous fluorescent signals. Complete tissue transparency enables us to acquire three-dimensional (3D) images of craniofacial bone vasculature, osteogenesis utilizing various labeling strategies, thus to investigate the spatial relationship among different tissues during postnatal craniofacial development. We found out that during the early stage of postnatal development, craniofacial osteogenesis occurs throughout the entire craniofacial bones, including the periosteum, dura, bone marrow, and suture. After 3–4 weeks, craniofacial osteogenesis is gradually restricted to the suture region and remaining bone marrow space. Similarly, craniofacial bone vasculature gradually restricts to the suture region. Osteogenesis is spatially associated with vasculature during the entire postnatal development. Importantly, we demonstrated that in adult calvarial bones, Gli1+ mesenchymal stem cells were also spatially associated with the vasculature. These findings indicate that craniofacial bones share similar osteogenesis mechanism as the long bone despite their distinct osteogenic mechanisms. In addition, the PEGASOS tissue clearing method-based 3D imaging technique is a useful new tool for craniofacial research.

Keywords: tissue clearing, suture, craniofacial bone, vasculature, mesenchymal stem cells, PEGASOS

Introduction

Craniofacial bones are different from those of the trunk. The craniofacial bones develop primarily from the cranial neural crest and partially from paraxial mesoderm through intramembranous ossification [1,2]. Research on craniofacial bone development has been focused on embryonic stages [1,3]. Much less is known about their postnatal development. It has been proposed that embryonic craniofacial ossification starts from a central mesenchymal condensation, from which preosteogenic cells rapidly expand outward and differentiate into osteoblasts while blood vessels concomitantly penetrate the external avascular layer under proangiogenic stimuli such as EDN1 (endothelin 1), VEGF (vascular endothelial growth factor), and HIF (hypoxia-inducible factor) [1,4–7]. Later, osteogenesis is achieved by osteoblasts, which move radially outward in all directions after mesenchymal cell expansion is completed [8,9]. Usually, the migration of precursor cells terminates when they approach the suture, where a stop signal is received [1,10]. In such a model, osteogenesis occurs in a radial pattern originating in the central part of the calvarial bone. Angiogenesis/osteogenesis coupling is well established in long bone formation [11]. Blood vasculature invades the primary and secondary growth centers, mediating endochondral ossification. Unfortunately, due to a lack of effective visualization techniques, there is limited direct evidence supporting this theory in craniofacial postnatal development, especially on a large three-dimensional (3D) scale. Our understanding of angiogenesis during craniofacial bone development remains limited.

Once development is completed, craniofacial bones undergo physiological turnover and can regenerate upon injury. In recent studies, suture mesenchymal stem cells (SuMSCs), which are identifiable as Gli1+ or Axin2+ cells residing in craniofacial sutures, were shown to be the stem cells supporting craniofacial bone homeostasis and injury repair [12,13]. Although mesenchymal stem cell (MSC) populations supporting long bones of adult mice have been shown to be closely associated with blood vessels [14–16], studies based mostly on conventional histological sections

Departments of [1]Biomedical Sciences and [2]Restorative Sciences, College of Dentistry, Texas A&M University, Dallas, Texas.
[3]State Key Laboratory of Oral Diseases, West China College of Stomatology, Sichuan University, Chengdu, People's Republic of China.
[4]Children's Research Institute, UT Southwestern Medical Center, Dallas, Texas.
Departments of [5]Pediatrics, [6]Neuroscience, and [7]Neurology and Neurotherapeutics, UT Southwestern Medical Center, Dallas, Texas.

have proposed that craniofacial SuMSCs are not associated with the vasculature [13].

A number of tissue clearing techniques have emerged in recent years from the neuroscience community. By rendering the brain or other tissues transparent, 3D images can be acquired with a confocal or two-photon microscope without sectioning. Three-dimensional imaging based on tissue clearing techniques can, therefore, provide more comprehensive information for investigating tissue organization and interaction [17,18]. Our laboratory recently developed the Poly(Ethylene Glycol) Associated Solvent System (PEGASOS) tissue clearing technique. The PEGASOS method clears both soft and hard tissues, including bones and teeth, thereby making it possible for microscopy lasers to pass through intact 3D tissues or organs [19]. Also, the PEGASOS method preserves endogenous fluorescence very well [20,21]. Fluorescent signals within the tissue can thus be directly visualized with a two-photon or confocal microscope.

In the current study, we applied the PEGASOS tissue clearing technique to the study of postnatal craniofacial bone development. We demonstrated the close spatial association between osteogenesis and angiogenesis during mouse postnatal craniofacial bone development. We demonstrated that Gli1+ MSCs within sutures are also spatially associated with the osteogenesis of craniofacial bones and with enriched vasculature within the suture.

Materials and Methods

Animals

C57BL/6 mice (JAX 000664) were obtained from the Jackson Laboratory. *Gli1-CreERT2* (JAX 007913) mice were crossed with *Ai14* mice (JAX 007908) to generate *Gli1-CreERT2*; *Ai14* mice. *Cdh5-Cre* mice (JAX 006137) were crossed with Ai14 to generate *Cdh5-Cre*; *Ai14* mice. All animal experiments were approved by the Texas A&M University Institutional Animal Care and Use Committee in accordance with guidelines from the NIH/NIDCR.

Tamoxifen administration and calcein green labeling

Tamoxifen (T5648; Sigma-Aldrich) was dissolved in corn oil (C8267; Sigma-Aldrich) to a 20 mg/mL stock concentration. For induction, *Gli1-CreERT2*; *Ai14* adult mice (4–6 weeks of age) were injected intraperitoneally with tamoxifen solution at a daily dosage of 10 μL/g body weight for 2 days. Calcein green (190167; MP Biomedical) was dissolved in saline to 4 mg/mL. Mice were intraperitoneally injected with calcein green solution (20 μL/g body weight) 2 h before sacrifice.

PEGASOS tissue clearing method

PEGASOS tissue clearing was performed as previously described [20]. Mice were transcardially perfused with 50 mL 0.02% heparin phosphate-buffered saline (w/v) and 20 mL 4% PFA under general anesthesia. Samples were collected and fixed in 4% PFA overnight at room temperature. Bones were then immersed in 0.5 M EDTA (pH 8.0) (E9884; Sigma-Aldrich) solution at 37°C to decalcify for 4 days if needed. This step was followed by decolorization treatment with 25% (v/v in H_2O) Quadrol (122262; Sigma-Aldrich) solution for 1 day at 37°C to remove remaining blood heme. Serial delipidation was then performed at 37°C under constant shaking for 6 h in each of the following solutions: 30% tert-butanol (tB) solution, 50% tB solution, and 70% tB solution. Thirty percent tB solution was composed of 75% v/v H_2O, 22% v/v tB (360538; Sigma-Aldrich), and 3% v/v Quadrol. Fifty percent tB solution was composed of 50% v/v H_2O, 47% v/v tB, and 3% v/v Quadrol. Seventy percent tB solution was composed of 30% v/v H_2O, 67% v/v tB and 3% v/v Quadrol. Samples were then dehydrated in tB-PEG solution composed of 75% tB, 22% (v/v) poly(ethylene glycol) methyl ether methacrylate average Mn500 (PEG MMA500; 447943; Sigma-Aldrich), and 3% (v/v) Quadrol at 37°C. Finally, samples were immersed in the benzyl benzoate (BB)-PEG clearing medium composed of 75% (v/v) BB (B6630; Sigma-Aldrich), 22% (v/v) PEG-MMA500, and 3% (v/v) Quadrol until transparency was achieved. Samples were preserved in the BB-PEG clearing medium at room temperature for storage and imaging. For bone samples collected for calcein green labeling, the clearing process was the same, except that the EDTA decalcification step was omitted.

Whole-mount immunofluorescent staining with laminin antibody

After decolorization with 25% Quadrol solution, samples were incubated in the blocking solution for 1 day at room temperature. The staining solution consisted of 10% v/v dimethyl sulfoxide (DMSO; w387520; Sigma-Aldrich), 0.5% w/v Igepal630 (I3021; Sigma-Aldrich), and 10% v/v 10× Casein blocking solution (SP5020; Vector) in phosphate-buffered saline (PBS; P4417; Sigma-Aldrich) solution. Samples were then incubated with laminin antibody conjugated with Alexa-488 (PA5-22901; Thermo Scientific) at 1:100 dilution for 5 days at room temperature on a shaker. Next, samples were washed with PBS at room temperature for 1 day. PBS was changed every 8 h. After the staining, clearing was resumed by placing samples into the tB delipidation solutions.

3D imaging and image analysis

After clearing, transparent samples were stored in the BB-PEG clearing medium within a cassette covered with glass. Three-dimensional images were acquired with a Zeiss LSM 780 two-photon microscope. Bone was outlined by Second Harmonic Generation (SHG), and calcein green or laminin-incorporating Alex 488 signal was imaged by two photons with 950 nm pulsed near infra red (NIR) excitation with a Zeiss BiG two-channel nondescanned detector. A 10×/0.45NA objective or 20×/0.85NA objectives were used for imaging. All raw image data were collected in 8-bit TIFF format. A 3D rendering of the image stacks was performed with Imaris 9.0 software (Bitplane). Bone marrow space located between cortical bones can be revealed by using ''clipping plane'' function module.

3D analysis

ImageJ (NIH) [22] was used for 3D quantification of vascular density and osteogenic activity. Vascular density was defined as the ratio of tdTomato-positive signal area to the total area of regions of interest (ROIs). The osteogenic activity was measured as the percentage of calcein green-positive signal area within the ROIs. The compiled Z stacks of vasculature and calcein green

(osteogenesis) images were converted to 8-bit Grayscale in ImageJ. Optical density (OD) was inverted using the command ''Edit>Invert'' and the background OD value was set to 0. Positive signal was highlighted by setting the threshold through ''Analyze>set scale.'' The positive signal area within each ROI was measured using the ''Analyze>set measurement'' function. For each sample, 12 ROIs were randomly selected with 4 from the suture region, 4 from the central region of the parietal bone, and the remaining 4 from the bone marrow space. Bone marrow space was identified by their porous morphology distinct from sutures or cortical bones. Signal within the bone marrow space was outlined and analyzed with Imaris 9.0 software.

Quantification and statistical analysis

Data were presented as mean ± standard error of mean. Statistical analysis was performed in IBM SPSS Statistics (version 21) using one-way analysis of variance with Bonferroni multiple comparisons test. With Bonferroni correction, $P < 0.0083$ was considered to be statistically significant.

Results

PEGASOS tissue clearing method rendered craniofacial bones transparent

Various craniofacial bones of interest were harvested (Fig. 1b–e1) and processed using the PEGASOS method, including fixation, decalcification (optional), decolorization, delipidation, dehydration, and clearing. A typical PEGASOS passive immersion procedure takes 1 week to finish. However, to investigate osteogenesis, decalcification is not needed so the total processing time can be shortened to 2–3 days (Fig. 1a). After clearing with decalcification, the calvaria, frontal bone, palate, and mandible turned transparent or invisible; even the teeth could be turned into fully transparent (Fig. 1b–e2). The grids in the background could be clearly seen through the cleared tissues. Without decalcification, craniofacial bones turned partially transparent after PEGASOS (Fig. 1b–e3). The resulting transparency enabled us to investigate craniofacial bone through 3D deep imaging.

Postnatal craniofacial osteogenesis was gradually restricted to the suture region and bone marrow space

Calcein green labeling was performed to evaluate osteogenesis. C57BL/6 mice were injected with calcein green on postnatal day 1 (P1), P7, P14, and P21. Calcein green fluorochrome can be incorporated into the matrix of osteogenic sites through chelation and enables visualization of newly formed bone [23]. The calvaria, frontal bone, and palate were isolated and cleared using the PEGASOS method without decalcification. Samples were imaged with a 10×0.45 objective on two-photon microscope. Calcein green signal was visualized in green channel and SHG signal was used to visualize bone. Two-dimensional (2D) images of coronal sections of calvarial bones were acquired to show details under 20× objectives on confocal microscope.

At P1, strong calcein green signal was detected throughout the calvarial bone, including surfaces underneath the

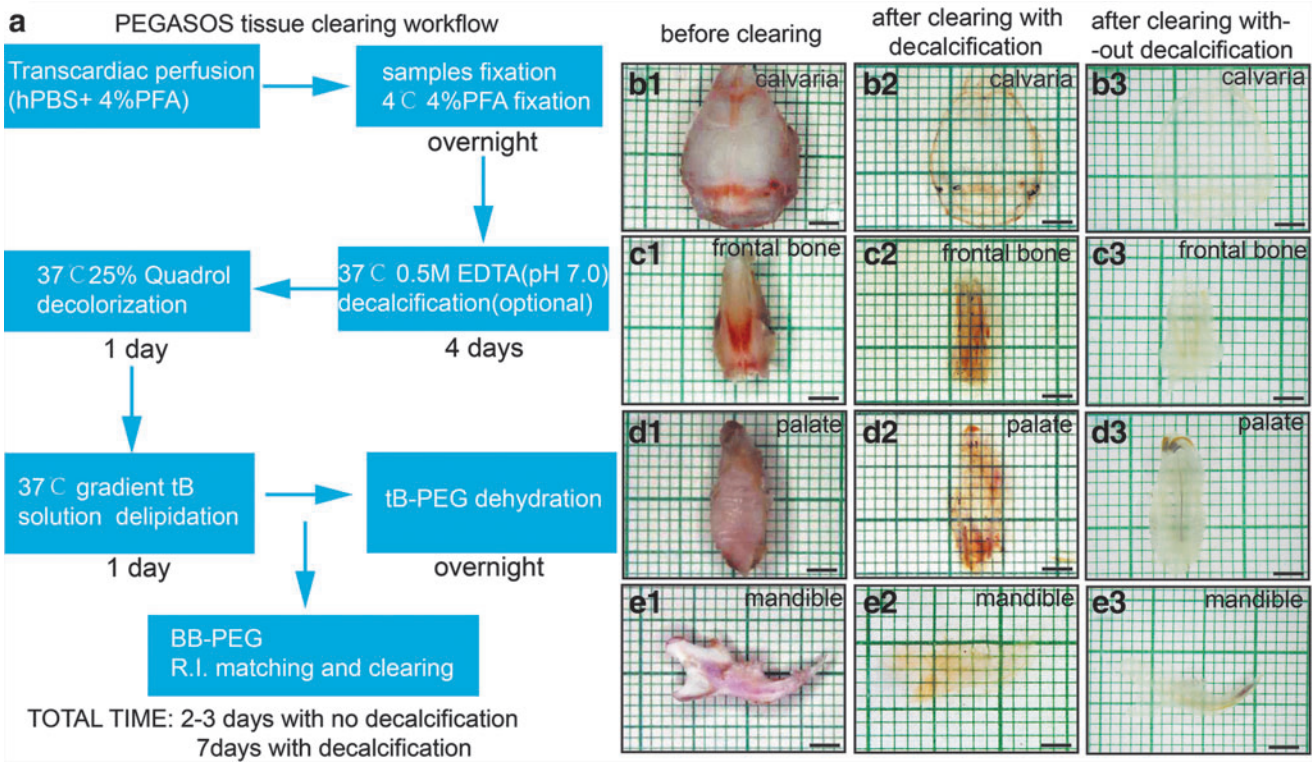

FIG. 1. PEGASOS tissue clearing method rendered craniofacial bones transparent. **(a)** Brief description of the PEGASOS tissue clearing procedure. Images of calvarial bone **(b1–b3)**, frontal bone **(c1–c3)**, palate **(d1–d3)**, and mandible **(e1–e3)** before and after clearing with the PEGASOS decalcification method or nondecalcification method. Scale bars, 2 mm. PEGASOS, Poly(Ethylene Glycol)Associated Solvent System.

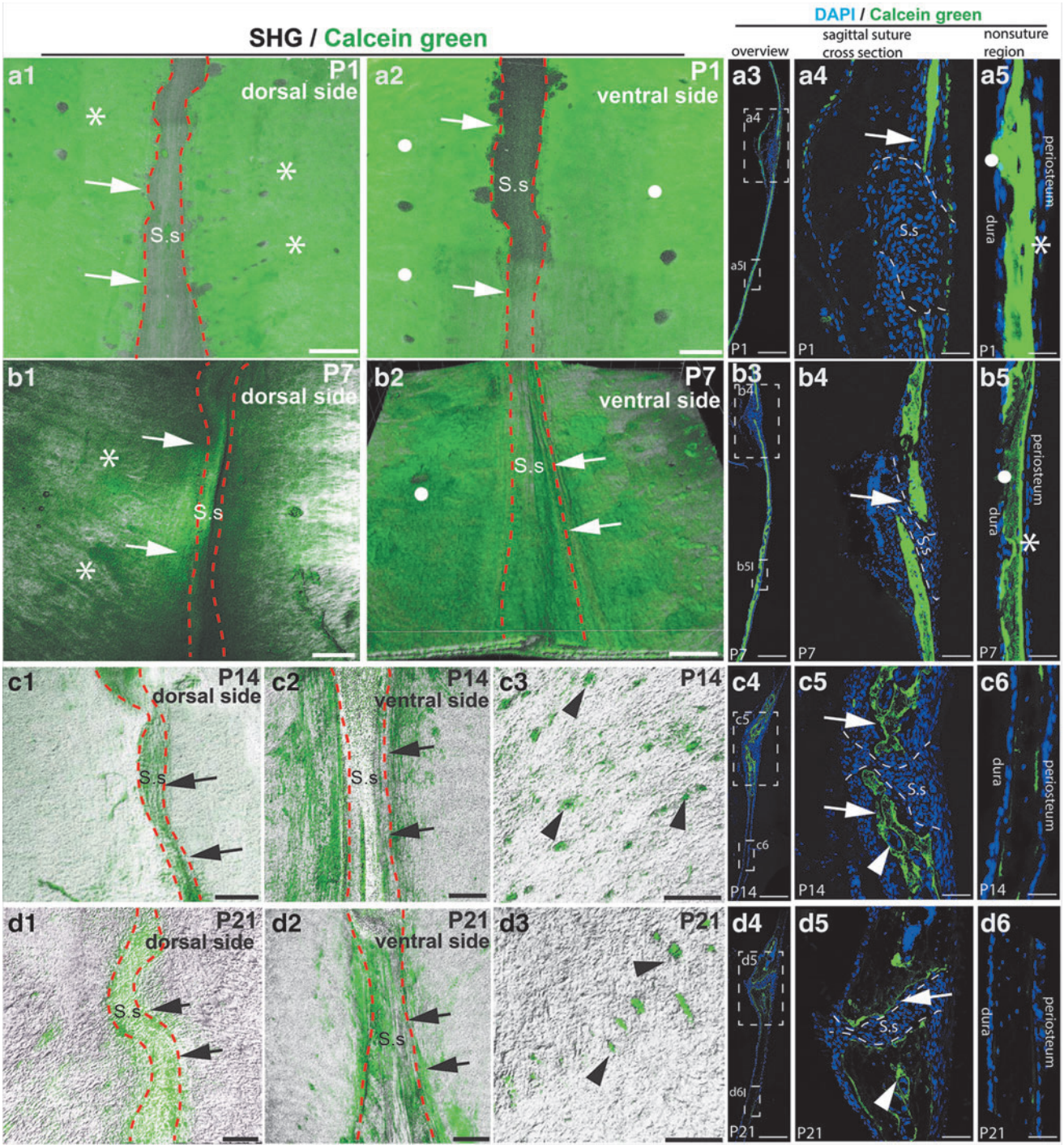

FIG. 2. Osteogenesis of parietal bone is gradually restricted to the suture and bone marrow regions during postnatal development. Calvarial bones were collected from mice at age of P1, P7, P14, or P21. Calcein green injection was performed 2 h before sacrifice. Three-dimensional imaging or histological sectioning was performed. *Green*, calcein green signal. *White*, SHG signal from the bone. *Blue*, DAPI staining. **(a1, a2)** Dorsal **(a1)** and ventral views **(a2)** of the calvarial bone of P1 mouse pups. **(a3–a5)** Histological sections of P1 sagittal suture. *Boxed* regions in **(a3)** were enlarged in **(a4, a5)** respectively. **(b1, b2)** Dorsal **(b1)** and ventral views **(b2)** of calvarial bones of P7 mouse pups. **(b3–b5)** Histological sections of P7 sagittal suture. *Boxed* regions in **(b3)** were enlarged in **(b4, b5)** respectively. **(c1, c2)** Dorsal **(c1)** and ventral views **(c2)** of the sagittal suture of P14 mice. **(c3)** The optical section at the calvarial bone center region was acquired to reveal calcein green within the bone marrow space (*arrowheads*). **(c4–c6)** Histological sections of the sagittal suture of P14 mice. *Boxed* regions in **(c4)** were enlarged in **(c5, c6)**, respectively. **(d1, d2)** Dorsal **(d1)** and ventral view **(d2)** of the sagittal suture of P21 mouse. **(d3)** The optical section was acquired to reveal calcein green within the calvarial bone marrow space (*arrowheads*). **(d4–d6)** Histological sections of P21 sagittal suture. *Boxed* regions in **(d4)** were enlarged in **(d5, d6)**, respectively. *Asterisks* indicate the calcein green signal underneath the periosteum. *Round dots* indicate calcein green signal underneath the dura. *Arrows* indicate signal surrounding the sagittal suture. *Dotted lines* outline sagittal sutures. S.s, sagittal suture. Scale bars, 50 μm in **(a4, a5, b4, b5, c5, c6, d5, d6)**; 100 μm in other *panels*. 3D, three-dimensional; SHG, Second Harmonic Generation.

periosteum (asterisks in Fig. 2a1, a5, and a3) or dura (dots in Fig. 2a2, a5, and a3,) and regions along the sagittal suture (arrows in Fig. 2a1, a2, a4, and a3). Relatively low calcein green signal was detected within the suture. Similarly, at p7, strong calcein green signal was detected over the entire calvarial bone under the periosteum (asterisks in Fig. 2b1, b5, and b3), dura (dots in Fig. 2b2, b5, and b3), and along the suture (arrows in Fig. 2b1, b2, b4, and b3). At p14, calcein green signal was restricted along the suture region (arrows in Fig. 2c1, c2, c5, and c4), but is much less underneath the periosteum or dura (Fig. 2c6). Optical sections showed positive signal also in the bone marrow space (arrowheads in Fig. 2c3, c5, and c4). At p21, calcein green signal was mostly detected along the suture (arrows in Fig. 2d1, d2, d5, and d4) and bone marrow space (arrowheads in Fig. 2d3, d5, and d4), but was absent from the underneath periosteum or dura (Fig. 2d6).

We also investigated osteogenic activity on the palatal and frontal bones. At p1 and p7, strong calcein green signal was visualized throughout the palatal and frontal bones, including the parasuture region (arrows) and bone marrow space (arrowheads) (Fig. 3a, b, e, f). At p14 and p21, strong calcein green signal was mostly detected along the suture (arrows) and within the bone marrow space (arrowheads), but was significantly reduced from other regions (Fig. 3c, d, g, h).

These indicated that osteogenic activity occurs widely throughout the calvarial bone immediately after birth, but gradually restricted to regions along the suture and bone marrow space.

Calvarial vasculature gradually restricted to the suture and bone marrow space regions between p7 and p14 after birth and were closely associated with osteogenic activity

Next, we investigated the vasculature distribution on the calvarial bone during the postnatal development by using *Cdh5-Cre*; *Ai14* mice. Vascular endothelial-cadherin (Cdh5) is a specific marker for labeling blood vessel endothelial cells [24]. Calvarial bones were harvested from C*dh5-Cre*; *Ai14* mice of P7 or P14 age and cleared following the PEGASOS method without decalcification. At p7, plenty of blood vessels were visualized throughout the calvarial bone, including the central part, the peripheral, and the suture region (Fig. 4a–a3). We did not notice significant differences in vascular density in different areas, including the suture region, central parietal bone, or bone marrow space (Fig. 5c). At p14, enriched vasculature remained within the suture region and peripheral bone marrow space (Fig. 4b–b4). Much fewer blood vessels were detected in the central part of the calvarial bone (Figs. 4b, b2, 5c). Blood vessels at the central calvarial bone region are all within the dura.

Calcein green incorporation assay was performed for *Cdh5-Cre*; *Ai14* mice of p7 or p14 age. At p7, strong calcein green was detected throughout the calvarial bone. Signal intensity was slightly higher in the suture region than the parietal bone center or peripheral bone marrow space regions (Fig. 5a–a2, d). TdTomato and calcein green signal highly colocalized with each other in either bone marrow space or suture region (Fig. 5a1, a2). At p14, calcein green signal still remained strong in the suture and peripheral bone marrow space regions but reduced dramatically in the central calvarial bone region (Fig. 5b–b3, d). TdTomato and calcein green signals remained colocalized with each other within the suture and peripheral bone marrow regions. Little calcein green signal colocalized with dura blood vessels in the central part of the calvarial bone (Fig. 5b1).

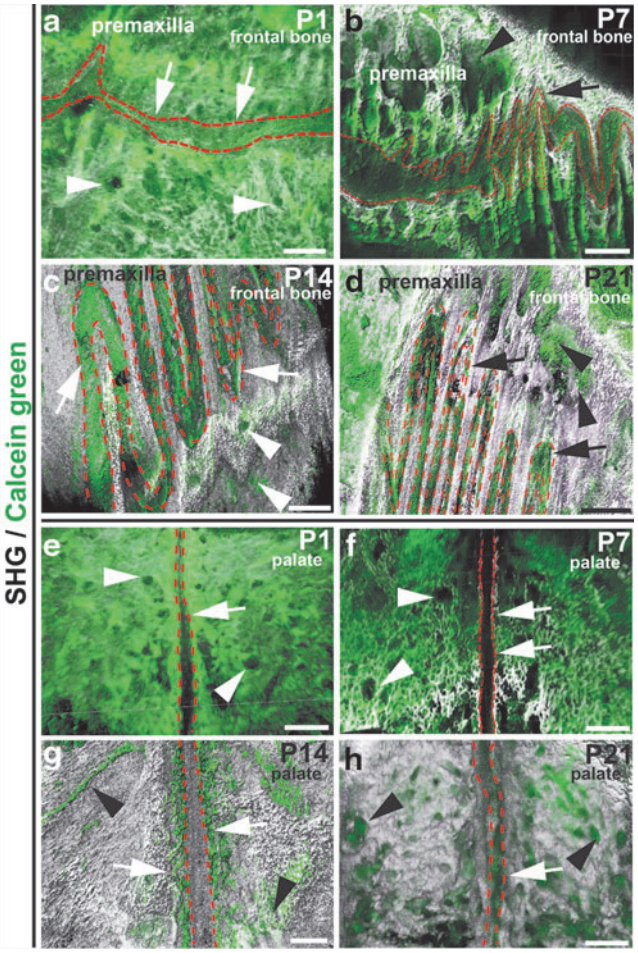

FIG. 3. Osteogenesis within the frontal and palatal bone is gradually restricted to suture regions and bone marrow space during postnatal development. Frontal **(a–d)** and palatal bone **(e–h)** samples were collected from mice at P1, P7, P14, or P21. Calcein green injection was performed 2 h before sacrifice. 3D images were acquired with a two-photon microscope after PEGASOS clearing treatment without decalcification. *Green*, calcein green signal. *White*, SHG signal from the bones. Osteogenic activity of the frontal and neighboring premaxillary bones harvested from mice of P1 **(a)**, P7 **(b)**, P14 **(c)**, or P21 **(d)** age. Osteogenic activity of the palatal bones harvested from mice of P1 **(e)**, P7 **(f)**, P14 **(g)**, or P21 **(h)** age. *Dotted lines* outline sutures. *Arrows* indicate the calcein green signal in the suture regions. *Arrowheads* indicate calcein green signal within the bone marrow space. Scale bars, 200 μm.

Osteogenic activity and calvarial vasculature are more restricted in suture and bone marrow space regions at the age of p21 and adult

We investigated the vasculature distribution on the calvarial bone in mice of P21 by using *Cdh5-Cre*; *Ai14* mice. Three-dimensional imaging indicated that at P21, vasculature within the suture still remained at similar density as in

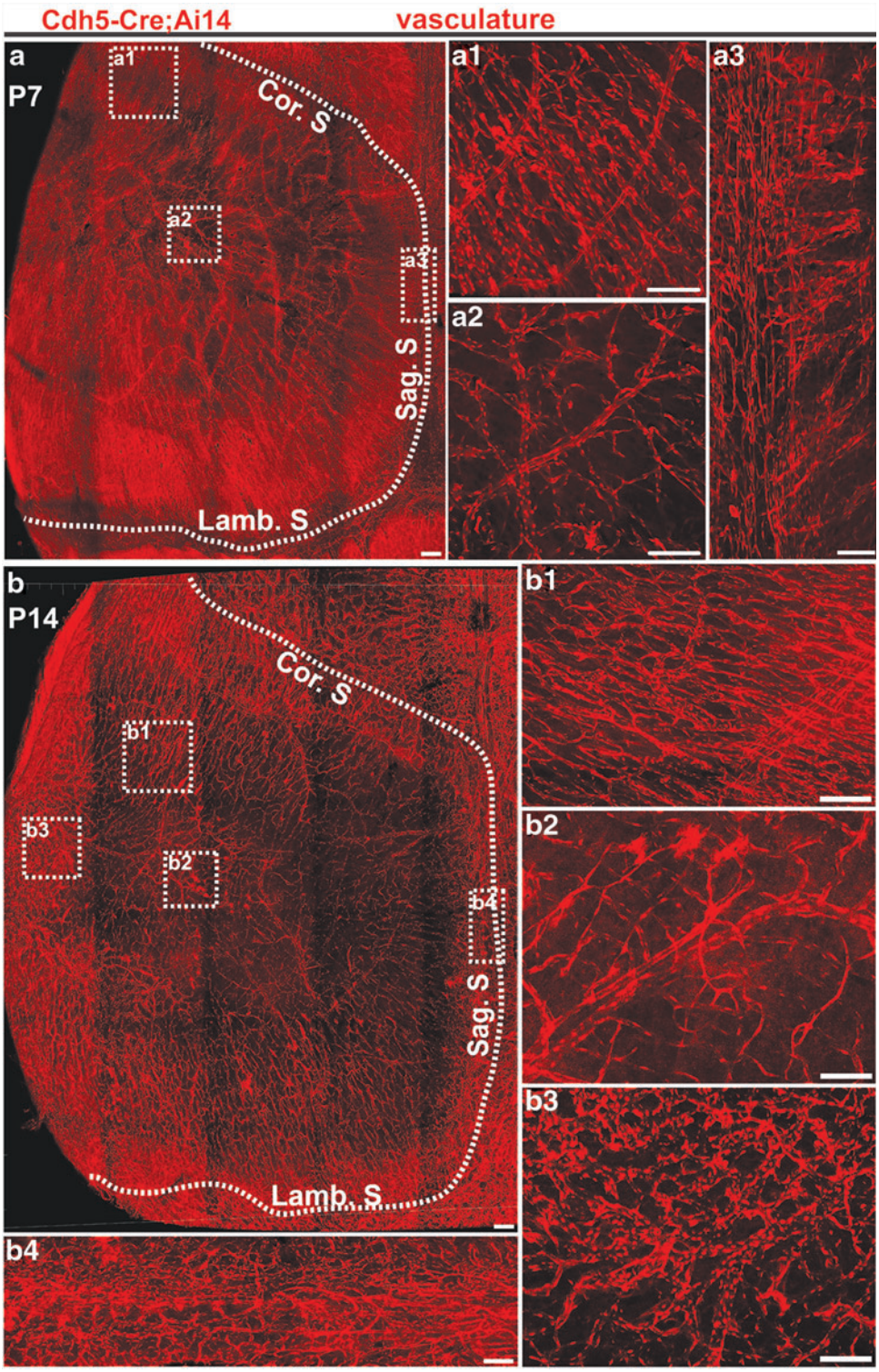

FIG. 4. Calvarial bone vasculature distribution pattern at P7 and P14. Calvarial bones were collected from *Cdh5-Cre; Ai14* mice at P7 or P14 and processed following the PEGASOS clearing method without decalcification. **(a)** Calvarial bone vasculature at age of P7. *Boxed* regions were enlarged in **(a1–a3)** as indicated. **(b)** Calvarial bone vasculature at P14 age. *Boxed* regions were enlarged in **(b1–b4)** as indicated. The *dotted line* outlines calvarial bones. Cor. S, coronal suture; Lamb. S, lambdoid suture; Sag. S, sagittal suture. Scale bars, 100 μm.

the younger mice (Fig. 6a, d′, and 6f compared with Fig. 5c). Calcein green assay indicated strong osteogenic activity along the suture, but at less intensity than in younger mice (Fig. 6a, d, and 6g compared with Fig. 5d). Bone marrow vasculature presented a reduced density than in younger mice (Fig. 6a, b′, and 6f compared with Fig. 5c). Calcein green signal was detected to be spatially associated with the bone marrow vasculature, but at a lower intensity than in younger mice (Fig. 6a, b, and 6g compared with Fig. 5d). Only a few blood vessels were detected in the central calvarial bone region, which is located within the dura. Little calcein green signal was detected along the dura vasculature (Fig. 6e–g).

Similar vasculature distribution was present in the calvarial bone of adult mice (6–8 weeks). The highest vasculature density was shown to be in the suture region. Calvarial peripheral bone marrow regions also had relatively enriched

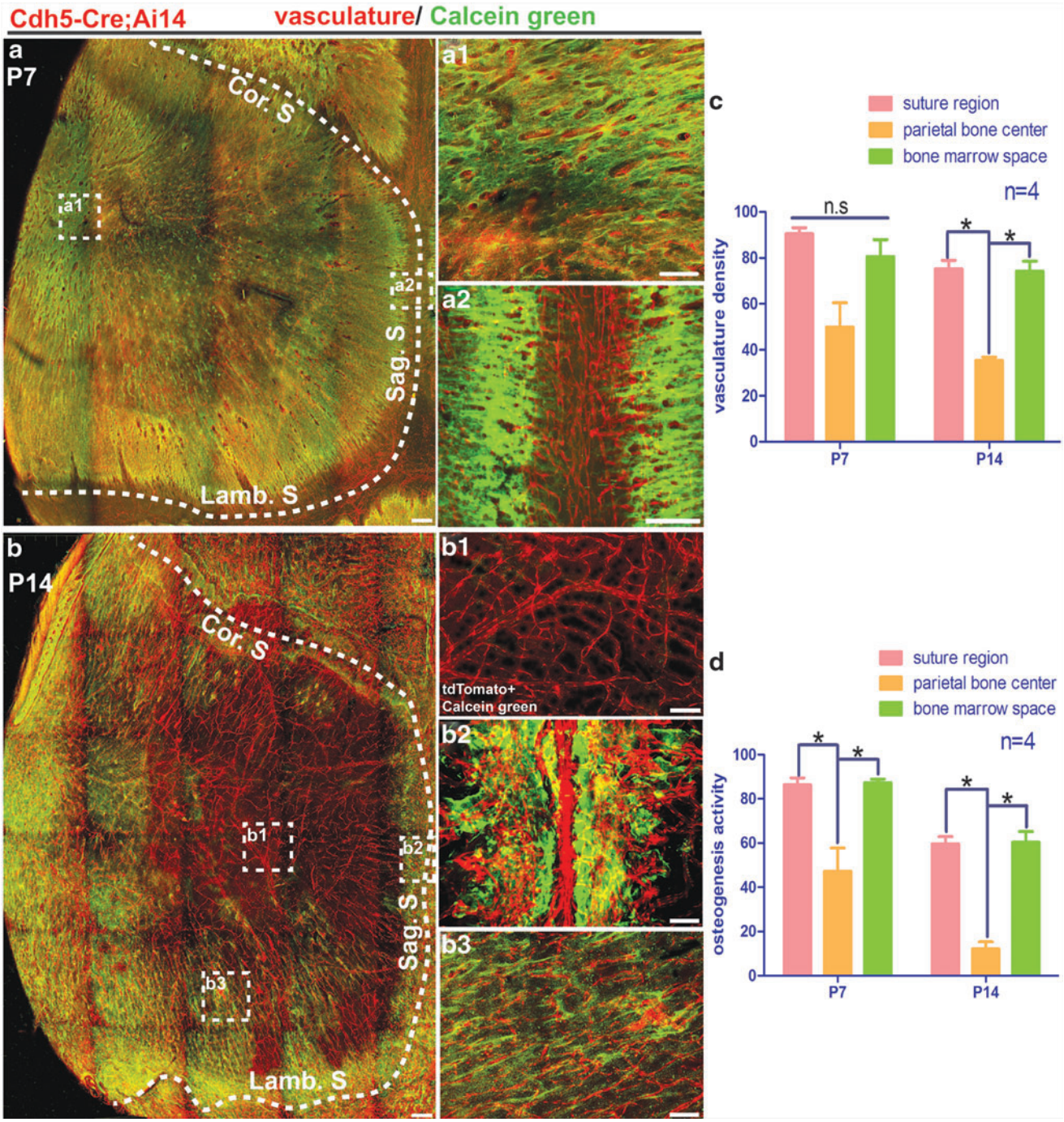

FIG. 5. Spatial association of osteogenesis with vasculature in calvarial bone during the first 2 weeks after birth. Calcein green injection was performed before sacrificing mice. Three-dimensional images were acquired with a two-photon microscope. **(a)** Distribution of vasculature (*red*) and calcein green signal (*green*) in the calvarial bone at the age of P7. The *dotted line* outlines calvarial bone. *Boxed* regions were enlarged in **(a1, a2)** as indicated. **(b)** Distribution of vasculature (*red*) and calcein green signal (*green*) in the calvarial bone at the age of P14. The *dotted line* outlines calvarial bone. *Boxed* regions were enlarged in **(b1–b3)** as indicated. Vascular density and osteogenic intensity at different locations were quantified in **(c, d)**. $^*P < 0.0083$. Cor. S, coronal suture; Lamb. S, lambdoid suture; n.s., no significant difference; Sag. S, sagittal suture. Scale bars, 100 μm.

blood vessels (Fig. 7a). Vasculature densities in suture and bone marrow were lower compared with mice of P21 age (Fig. 7d compared with Figs. 5c and 6f). Few blood vessels were detected in the central calvarial bone region (Fig. 7a, d). Calcein green signal was detected along the suture and the bone marrow space regions with lower intensities than in younger mice (Fig. 7e compared with Figs. 5d and 6g). Calcein green signal associated closely with the vasculature (Fig. 7b, c). Little calcein green signal was detected in the central calvarial bone region (Fig. 7a, e).

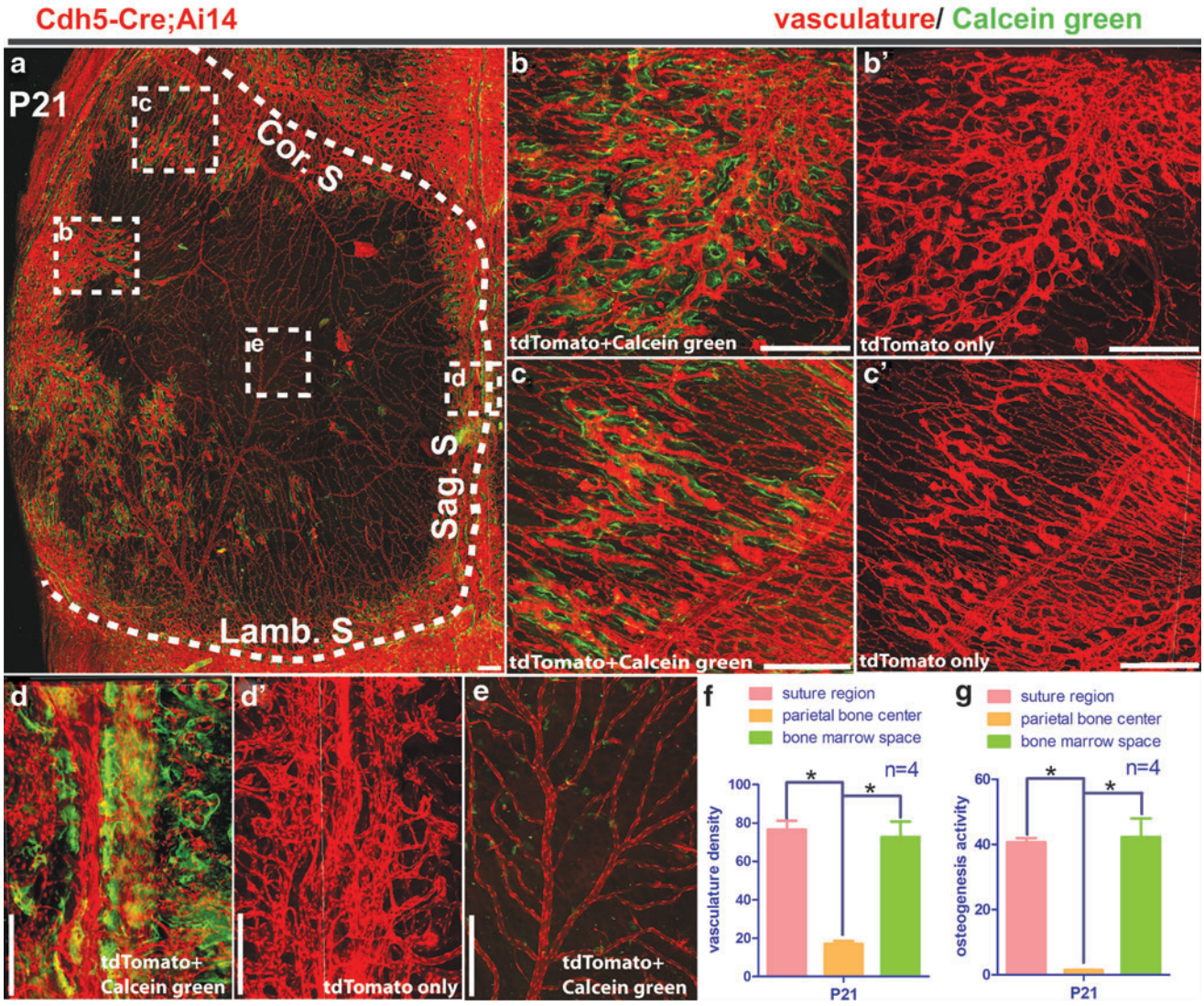

FIG. 6. Spatial association of vasculature with osteogenesis in mouse calvarial bone at P21. Calvarial bones were collected from *Cdh5-Cre; Ai14* mice at P21. Calcein green injection was performed before sacrificing mice. Samples were cleared following the PEGASOS method without decalcification. **(a)** Maximum project view of the vasculature (*red*) and calcein green signal (*green*) in the calvarial bone. *Boxed* regions were enlarged in **(b, b′, c, c′, d, d′** and **e)** as indicated. The *dotted line* outlines calvarial bone. Vascular densities and calcein green signal intensities at different locations on the calvarial bone were quantified in **(f, g)**. $*P < 0.0083$. Cor. S, coronal suture; Lamb. S, lambdoid suture; Sag. S, sagittal suture. Scale bars, 250 μm.

These results indicated that calvarial vascular density gradually reduced and vasculature was restricted to the suture and peripheral bone marrow regions after p21 and in the adult. The osteogenic activity was closely associated with blood vessels within the suture and peripheral bone marrow regions but was not associated with dura vasculature.

In adult mice, Gli1+ SuMSCs were closely associated with vasculature and craniofacial osteogenesis

Gli1+ cells within the suture are MSCs supporting craniofacial bone turnover and injury repair [13,25]. Previous studies based on conventional 2D imaging concluded Gli1+ cells were not associated with the vasculature. To investigate relationships between Gli1+ MSCs with osteogenesis and vasculature, we generated *Gli1-Cre^{ERT2}*; *Ai14* model and induced with tamoxifen for adult mice (6–8 weeks) to label Gli1+ cells in adult sutures. In combination with calcein green labeling and the PEGASOS tissue clearing techniques, we were able to elucidate the relationship between MSCs and osteogenesis through 3D imaging following the protocol shown in Fig. 8a. Sagittal, palatal, and frontal/premaxilla sutures were isolated and processed with the PEGASOS method without decalcification. The 3D imaging indicated Gli1+ cells distributed exclusively within sutures. Osteogenic sites uniformly appeared adjacent to Gli1+ SuMSCs in the sagittal suture, palatal suture, and frontal/premaxilla suture (Fig. 8b–d).

To investigate the spatial relationship between Gli1+ MSCs and vasculature, laminin whole-mount staining was performed to label vasculature within the sagittal suture and the nearby blood vessel loops, as indicated in Fig. 8f. Adult

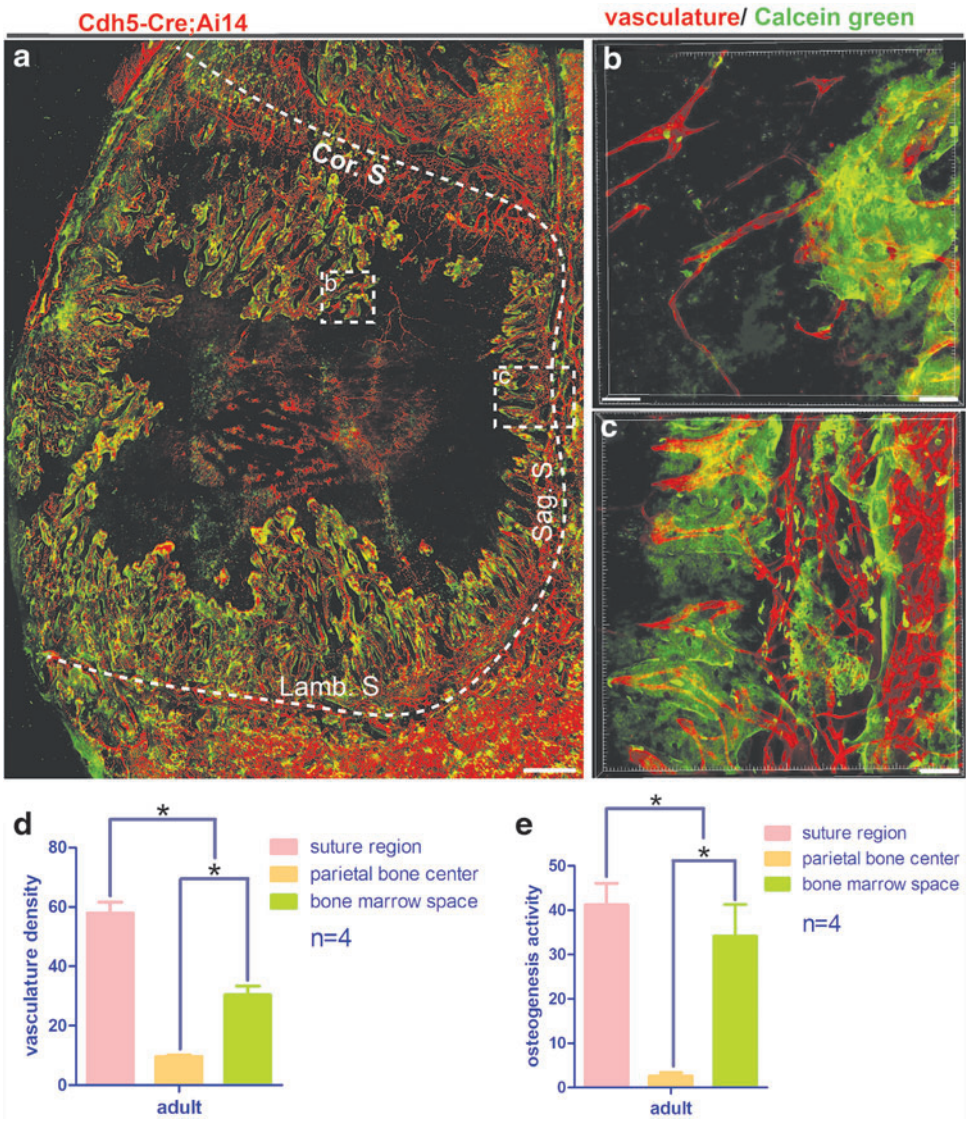

FIG. 7. Spatial association of vasculature with osteogenesis in adult mouse calvarial bone. Calcein green injection was performed for adult *Cdh5-Cre; Ai14* mice (6–8 weeks age) before sacrifice. Samples were processed using the PEGASOS method and imaged with a two-photon microscope. **(a)** Maximum project view of the vasculature (*red*) and calcein green (*green*) in the calvarial bone. The *dotted line* outlines calvarial bone. *Boxed* regions were enlarged in **(b, c)** as indicated. Vascular densities and calcein green signal intensities at different locations on the calvarial bone were quantified in **(d, e)**. $*P < 0.0083$. Scale bars, 200 μm. Cor. S, coronal suture; Lamb. S, lambdoid suture; Sag. S, sagittal suture.

Gli1-Cre^{ERT2}; *Ai14* mice were used to label Gli1+ MSCs after 4 days of induction with tamoxifen. The calvarial bone then underwent the PEGASOS method with decalcification as described in Fig. 8e. Interestingly, 3D imaging indicated that Gli1+ cells within the suture were surrounding the vasculature (Fig. 8g, h).

Taken together, 3D imaging revealed that Gli1+ cells within the suture are spatially associated with osteogenic activity in adult craniofacial bones and are also adjacent to the vasculature.

Discussion

Craniofacial bones are flat bone originating mostly from the cranial neural crest cells of ectoderm and partially from mesoderm. Intramembranous osteogenesis is the dominant process during craniofacial bone formation. In contrast, long bones in the trunk region were derived from mesoderm and governed mainly by endochondral osteogenesis. Endochondral osteogenesis process in long bone development has been shown to be closely associated with the vasculature. Osteogenic progenitor cells were proposed to migrate along and regulated by blood vessels. Coupling between angiogenesis and osteogenesis is a critical process during long bone development and regeneration [26,27]. Intramembranous osteogenic procedure during the craniofacial bone development was much less understood, especially during the postnatal development stage [28]. It remains largely unknown if craniofacial osteogenesis during postnatal development is coupled with vasculature development. The complicated shape and organization of craniofacial organs constitute a challenge for visualizing and investigating their vasculature organization and development. By using the PEGASOS clearing method-based 3D imaging combining with transgenic mouse model for labeling endothelium, we were able to visualize the spatial organization of craniofacial vasculature. Our results provided direct evidence that the craniofacial osteogenic process is also coupled with vasculature throughout the entire postnatal craniofacial development. In the first 2 weeks after birth, strong osteogenesis and enriched vasculature were visualized throughout the entire craniofacial bones. After P14, osteogenic activity and vasculature density

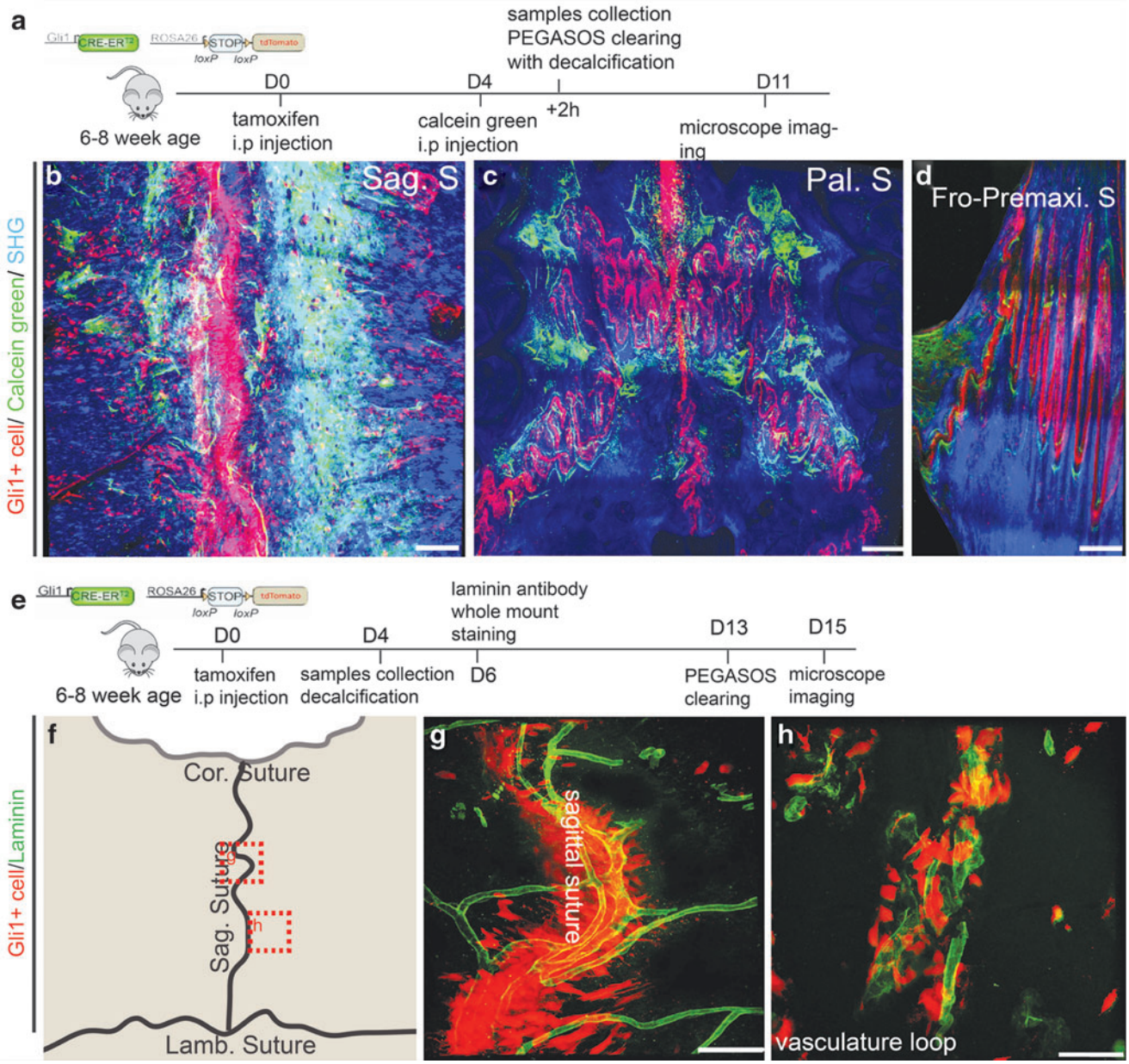

FIG. 8. In adult mice, Gli1+ MSCs within the suture are spatially associated with osteogenesis and vasculature. **(a)** Experimental design for labeling Gli1+ cells using *Gli1-CreERT2; Ai14* mice and for labeling osteogenesis with calcein green injection. **(b)** Association of Gli1+ cells (*red*) with osteogenic activity (*green*) within the sagittal **(b)**, palatal **(c)**, and frontal/premaxilla **(d)** sutures. **(e)** Experimental design for labeling Gli1+ cells using *Gli1-CreERT2; Ai14* mice and for labeling vasculature with laminin antibody. **(f)** Schematic drawing of calvarial bone showing the image locations of *panel* **(g, h)**. **(g, h)** A 3D image stack of 100 μm thickness showed the spatial association of Gli1+ cells (*red*) with the vasculature (*green*) within **(g)** and near **(h)** the sagittal suture. Cor. S, coronal suture; Fro-Premaxi. S, frontal/premaxilla suture; Lamb. S, lambdoid suture; MSCs, mesenchymal stem cells; Sag. S, sagittal suture. Scale bars, 100 μm.

reduced significantly and both are more enriched in the suture and bone marrow space regions.

Blood vessels on the calvarial bone can be categorized into three distinct types based on their locations, within sutures, bone marrow space, or dura. We did not detect vasculature within the calvarial bone periosteum. Dura vasculature density significantly reduces during postnatal development and is not associated with osteogenesis after p14. Bone marrow vasculature density also significantly reduces during postnatal development but is always associated with osteogenesis. Suture vasculature remains highly enriched even in adult mice is always associated with osteogenesis. The coupling between osteogenesis and vasculature suggests potential interactions and regulations between osteogenic mesenchymal cells and blood vessel components of craniofacial bones. Perivasculature has been proposed to be the stem cell niche for numerous mesenchymal organs [29–32]. Craniofacial sutures in adult mice were known to be the niche for craniofacial MSCs supporting bone turnover and injury repair. These SuMSCs, which could be labeled by *Gli1* or *Axin2* expression [12,13],

were located at the midline of the suture mesenchyme. They are negative for osteogenic differentiation markers and can give rise to osteoblast located within the osteogenic fronts and osteocytes within the craniofacial bones. Maintenance of SuMSCs are essential for suture patency, and ablation of these MSCs led to suture fusion. Differentiation of these SuMSCs were regulated by IHH secreted from the osteogenic front [13]. Although perivascular niche was known to be critical for many MSC populations, based on 2D sections, it was proposed that SuMSCs are not related to blood vessels [13]. Our 3D imaging results disapproved the above conclusion. Enriched blood vessels remain within the calvarial bone suture of adult mice and are spatially associated with osteogenic activity and Gli1+ MSCs. Like MSCs of the long bone, Gli1+ MSCs of craniofacial bones are also perivascular located.

In summary, our study indicated that PEGASOS tissue clearing-based 3D imaging is a useful tool for investigating craniofacial bone development and MSCs. We showed that craniofacial osteogenesis is spatially associated with the vasculature during postnatal development. SuMSCs of craniofacial bones are also spatially associated with the vasculature.

Acknowledgments

The authors thank Kate Phelps and the UTSW Live Cell Imaging Facility for technical support with microscopy. They thank Bridget Samuels for critical reading of the article. They thank Ms. Meng Zhang and Ms. Evelyn Zhao for the support.

Author Disclosure Statement

A patent related to the PEGASOS clearing method used in the research has been submitted by W.L., D.J., S.Z., and H.Z. The others authors declare no conflicts of interest.

Funding Information

This work was supported by startup funding from Texas A&M University, National Institute of Health (NIH)/National Institute of Dental and Craniofacial Research (NIDCR) grant K08DE025090, R01 DE028291, and R21 DE027928 to H.Z.

References

1. Percival CJ and JT Richtsmeier. (2013). Angiogenesis and intramembranous osteogenesis. Dev Dyn 242:909–922.
2. Kish PE, BL Bohnsack, D Gallina, DS Kasprick and A Kahana. (2011). The eye as an organizer of craniofacial development. Genesis 49:222–230.
3. Thompson TJ, PD Owens and DJ Wilson. (1989). Intramembranous osteogenesis and angiogenesis in the chick embryo. J Anat 166:55–65.
4. Hall BK and T Miyake. (2000). All for one and one for all: condensations and the initiation of skeletal development. Bioessays 22:138–147.
5. Rice DP, T Aberg, Y Chan, Z Tang, PJ Kettunen, L Pakarinen, RE Maxson and I Thesleff. (2000). Integration of FGF and TWIST in calvarial bone and suture development. Development 127:1845–1855.
6. Filipowska J, KA Tomaszewski, L Niedzwiedzki, JA Walocha and T Niedzwiedzki. (2017). The role of vasculature in bone development, regeneration and proper systemic functioning. Angiogenesis 20:291–302.
7. von Schroeder HP, CJ Veillette, J Payandeh, A Qureshi and JN Heersche. (2003). Endothelin-1 promotes osteoprogenitor proliferation and differentiation in fetal rat calvarial cell cultures. Bone 33:673–684.
8. Lana-Elola E, R Rice, AE Grigoriadis and DP Rice. (2007). Cell fate specification during calvarial bone and suture development. Dev Biol 311:335–346.
9. Yoshida T, P Vivatbutsiri, G Morriss-Kay, Y Saga and S Iseki. (2008). Cell lineage in mammalian craniofacial mesenchyme. Mech Dev 125:797–808.
10. Opperman LA and JT Rawlins. (2005). The extracellular matrix environment in suture morphogenesis and growth. Cells Tissues Organs 181:127–135.
11. Ramasamy SK, AP Kusumbe and RH Adams. (2015). Regulation of tissue morphogenesis by endothelial cell-derived signals. Trends Cell Biol 25:148–157.
12. Maruyama T, J Jeong, TJ Sheu and W Hsu. (2016). Stem cells of the suture mesenchyme in craniofacial bone development, repair and regeneration. Nat Commun 7: 10526.
13. Zhao H, J Feng, TV Ho, W Grimes, M Urata and Y Chai. (2015). The suture provides a niche for mesenchymal stem cells of craniofacial bones. Nat Cell Biol 17:386–396.
14. Wang A, X Zhou, J Zhao, T Liu and J Xu. (2015). Therapeutic effects of bone marrow mesenchymal stem cells expressing interleukin-12 in mice bearing malignant ascites tumor. Int J Clin Exp Med 8:15840–15845.
15. Worthley DL, M Churchill, JT Compton, Y Tailor, M Rao, Y Si, D Levin, MG Schwartz, A Uygur, et al. (2015). Gremlin 1 identifies a skeletal stem cell with bone, cartilage, and reticular stromal potential. Cell 160:269–284.
16. Grayson WL, BA Bunnell, E Martin, T Frazier, BP Hung and JM Gimble. (2015). Stromal cells and stem cells in clinical bone regeneration. Nat Rev Endocrinol 11:140–150.
17. Acar M, KS Kocherlakota, MM Murphy, JG Peyer, H Oguro, CN Inra, C Jaiyeola, Z Zhao, K Luby-Phelps and SJ Morrison. (2015). Deep imaging of bone marrow shows non-dividing stem cells are mainly perisinusoidal. Nature 526:126–130.
18. Guldberg RE. (2009). Spatiotemporal delivery strategies for promoting musculoskeletal tissue regeneration. J Bone Miner Res 24:1507–1511.
19. Jing D, Y Yi, W Luo, S Zhang, Q Yuan, J Wang, E Lachika, Z Zhao and H Zhao. (2019). Tissue clearing and its application to bone and dental tissues. J Dent Res 98:621–631.
20. Jing D, S Zhang, W Luo, X Gao, Y Men, C Ma, X Liu, Y Yi, A Bugde, et al. (2018). Tissue clearing of both hard and soft tissue organs with the PEGASOS method. Cell Res 28: 803–818.
21. Yi Y, Y Men, D Jing, W Luo, S Zhang, JQ Feng, J Liu, WP Ge, J Wang and H Zhao. (2019). 3-Dimensional visualization of implant-tissue interface with the polyethylene glycol associated solvent system tissue clearing method. Cell Prolif 52:e12578.
22. Schneider CA, WS Rasband and KW Eliceiri. (2012). NIH Image to ImageJ: 25 years of image analysis. Nat Methods 9:671–675.

23. Ruehe B, S Heberer, K Bayreuther and K Nelson. (2011). Effect of dehiscences to the bone response of implants with an Acid-etched surface: an experimental study in miniature pigs. J Oral Implantol 37:3–17.
24. Vestweber D. (2008). VE-cadherin: the major endothelial adhesion molecule controlling cellular junctions and blood vessel formation. Arterioscler Thromb Vasc Biol 28:223–232.
25. Zhao H and Y Chai. (2015). Stem cells in teeth and craniofacial bones. J Dent Res 94:1495–1501.
26. Trueta J and AJ Buhr. (1963). The vascular contribution to osteogenesis. V. The vasculature supplying the epiphysial cartilage in rachitic rats. J Bone Joint Surg Br 45:572–581.
27. Kusumbe AP, SK Ramasamy and RH Adams. (2014). Coupling of angiogenesis and osteogenesis by a specific vessel subtype in bone. Nature 507:323–328.
28. Abzhanov A, SJ Rodda, AP McMahon and CJ Tabin. (2007). Regulation of skeletogenic differentiation in cranial dermal bone. Development 134:3133–3144.
29. Hopper RA, JR Zhang, VL Fourasier, I Morova-Protzner, KF Protzner, CY Pang and CR Forrest. (2001). Effect of isolation of periosteum and dura on the healing of rabbit calvarial inlay bone grafts. Plast Reconstr Surg 107:454–462.
30. Crisan M, S Yap, L Casteilla, CW Chen, M Corselli, TS Park, G Andriolo, B Sun, B Zheng, et al. (2008). A perivascular origin for mesenchymal stem cells in multiple human organs. Cell Stem Cell 3:301–313.
31. Zhao H, J Feng, K Seidel, S Shi, O Klein, P Sharpe and Y Chai. (2014). Secretion of shh by a neurovascular bundle niche supports mesenchymal stem cell homeostasis in the adult mouse incisor. Cell Stem Cell 14:160–173.
32. Kramann R, RK Schneider, DP DiRocco, F Machado, S Fleig, PA Bondzie, JM Henderson, BL Ebert and BD Humphreys. (2015). Perivascular Gli1+ progenitors are key contributors to injury-induced organ fibrosis. Cell Stem Cell 16:51–66.

Address correspondence to:
Hu Zhao, DDS, PhD
Department of Restorative Sciences
College of Dentistry
Texas A&M University
3302 Gaston Avenue
Dallas, TX 75246

E-mail: huzhao@tamu.edu

Received for publication May 12, 2019
Accepted after revision August 7, 2019
Prepublished on Liebert Instant Online August 8, 2019